Sensors and Actuators A 155 (2009) 1–7

Contents lists available at ScienceDirect

Sensors and Actuators A: Physical

journal homepage: www.elsevier.com/locate/sna

Microsystem for nanofiber electromechanical measurements☆

Joseph J. Brown[a,e,*], Ji Won Suk[b,e], Gurpreet Singh[c], Alicia I. Baca[a,e], Dmitriy A. Dikin[d,e], Rodney S. Ruoff[b,e], Victor M. Bright[a,e]

[a] University of Colorado - Boulder, Department of Mechanical Engineering, Boulder, CO 80309-0427, United States
[b] University of Texas - Austin, Department of Mechanical Engineering, Austin, TX 78712-0292, United States
[c] Virginia Polytechnic Institute and State University, Institute for Critical Technology and Applied Science, Blacksburg, VA 24061, United States
[d] Northwestern University, Department of Mechanical Engineering, Evanston, IL 60208, United States
[e] DARPA Center for Integrated Micro/Nano-Electromechanical Transducers (iMINT), University of Colorado - Boulder, Boulder, CO 80309-0427, United States

ARTICLE INFO

Article history:
Received 16 July 2008
Received in revised form 11 November 2008
Accepted 11 November 2008
Available online 19 November 2008

Keywords:
Electromechanical testing
Nanofiber
Uniaxial
Straining stage
Calibration

ABSTRACT

A microscale, thermally actuated, uniaxial testing stage for nanofiber materials has been designed and fabricated. Electrical separation of portions of the stage allows two-point electrical measurements simultaneously with *in situ* mechanical testing. Using this stage, a nanofiber consisting of a carbon nanotube (CNT) surrounded by amorphous carbon was subjected to mechanical loading and simultaneous electrical impedance characterization, which provides a means to derive fiber resistance measurements when a fiber is mechanically coupled using highly resistive contacts. Stress applied to the nanofiber was estimated using measurements of the stage displacement and the input power supplied to the thermal actuator.

1. Introduction

Electromechanical measurements of nanoscale fibers such as nanotubes and nanowires are of interest to enable integration of these materials into sensors and other microdevices [1,2]. Uniaxial loading is desirable in mechanical testing to ensure uniform loading throughout a fiber specimen [3,4], and to this end several microdevices have been developed to perform uniaxial mechanical testing on a nanofiber [5–11]. Furthermore, electrical coupling to a specimen can allow piezoresistive and electrothermomechanical characterization. The novelty of the device presented here lies in the ability to perform electrical measurement of an electrically conducting or semiconducting nanoscale fiber specimen under mechanical loading. This work also explores the use of alternating current (ac) electrical measurements as a novel means to bypass contact resistance in two-point electrical measurements of a fiber specimen mounted on a microsystem. This paper is an expansion of a paper presented at the 2008 Solid State Sensors, Actuators, and Microsystems Workshop in Hilton Head, SC, USA [12]. For mechanical tester microsystems such as those in references [5–11], measurement of the forces generated with the system remains a challenge. The current paper builds on Ref. [12] by including a demonstration of a new force calibration approach based on the discrepancy between expected and measured displacements.

2. Design and simulation

The MEMS tensile test system developed here consists of a moving stage and a fixed stage, as seen in Fig. 1. These components are built from released polysilicon using the PolyMUMPS prototyping service [13]. The fixed stage is anchored to a silicon nitride substrate, and the moving stage is connected by a shuttle to a thermal actuator, and it is stabilized to uniaxial motion by a set of opposing beams which are anchored at their ends to the nitride substrate.

2.1. Mechanical design

Stage actuation is realized by thermal expansion through Joule heating of a set of angled beams, as has been previously explored in Refs. [14–16]. Beams symmetrically connected to the stage ensure uniaxial motion and also serve as heat sinks. Using the actuator geometry and a plane strain condition in a solid mechanics mathematical analysis, the thermal actuator was estimated to provide up to 400 μN force output. The plane strain condition approximates the case where the stage is constrained not to move even as the beams in the actuator are forced to thermally expand due to Joule heating.

☆ This paper is part of the Special Section of the Micromechanics Section of Sensors and Actuators based on contributions revised from the Technical Digest of the 2008 Solid-State Sensors, Actuators and Microsystems Workshop sponsored by the Transducer Research Foundation, Inc. (1–5 June 2008, Hilton Head Island, South Carolina, USA).

* Corresponding author.
E-mail address: Joseph.J.Brown@colorado.edu (J.J. Brown).

0924-4247/$ – see front matter © 2008 Elsevier B.V. All rights reserved.
doi:10.1016/j.sna.2008.11.001

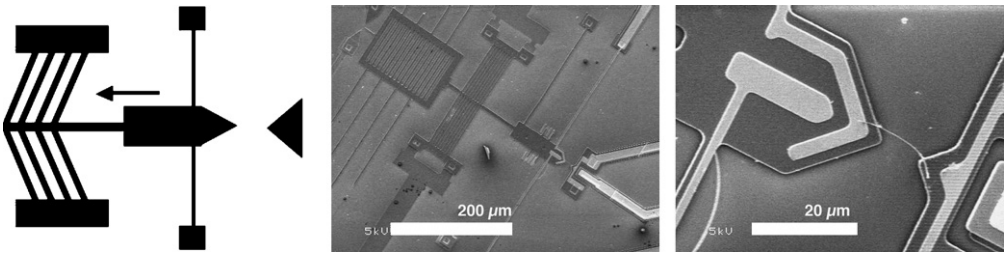

Fig. 1. Left: diagram of actuator and stage system. The moving stage at left is linked by bending beams to rectangular anchor points. A thermal actuator pulls the moving stage away from the fixed stage, at right. Center: SEM image of overall system. Right: close-up view of stage showing mounted carbon nanofiber, 120 nm diameter, before loading.

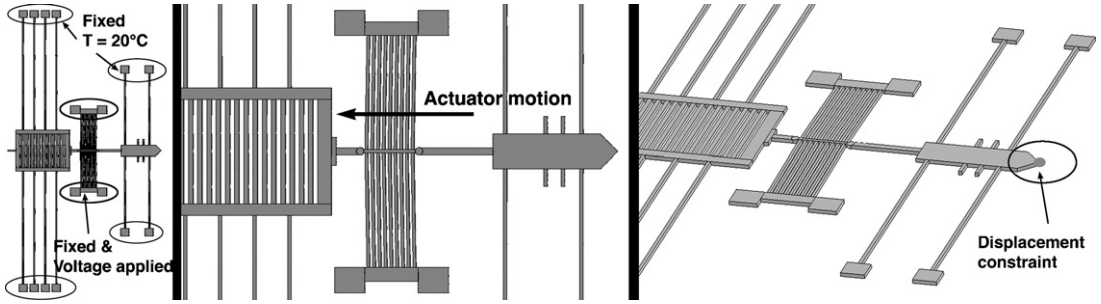

Fig. 2. Layout for simulation. The moving stage is the pointed part at the right of the device, the thermal actuator is at the center, and the springs and large grating at the left were added to test several indirect means of displacement measurement.

As electrical power is increased to the actuator, the heat flow out of the actuator increases. Because of the polysilicon thermal resistance, the temperature rises in the actuator due to the increased heat flow. The temperature increase causes thermal expansion of the silicon, which produces force if the motion of the expanding polysilicon beams is constrained. By angling the actuator beams 1° off of perpendicular to the shuttle that transmits force to the test stage, the expanding beams are made to cancel their off-axis motion, and they experience a buckling motion only in the shuttle axis.

Simulations were performed in order to define the behavior of the system across a range of applied input voltages. A preliminary simulation used the values in Table 1, the structure in Fig. 2, and a tetrahedral coupled-field element, SOLID98, in ANSYS 10.0 software. The simulation did not include the temperature dependence of polysilicon electrical and thermal conductivities. This simulation was repeated in COMSOL 3.4 multiphysics simulation software in order to check the results. The COMSOL simulation used 16,637 Quadratic Lagrange tetrahedral elements.

In order to estimate the force applied from the stage to a mounted nanofiber, a displacement boundary condition was assigned to the moving stage. When no displacement constraint is assigned, corresponding to the absence of a test specimen, the simulation provides a parabolic curve of displacement versus voltage, similar in shape to the measured behavior. If the displacement is plotted against the square of the voltage, which is proportional to the input power, a linear relation is evident between power and displacement, as seen in Fig. 3.

At fixed voltages, with varying displacement constraints, the moving stage exhibits a linear reaction force versus displacement. Force simulation as shown in Fig. 4 indicates the analytical estimate of 400 μN to be a reasonable order of magnitude for a zero micron displacement constraint. The actuator experimentally demonstrated >1.60 μm displacement, also in good agreement with the values estimated in Fig. 4.

2.2. Thermal design

In order to minimize the specimen temperature changes caused by the thermal actuator in Refs. [5,6], the moving stage was sepa-

Table 1
Polysilicon material properties used as simulation inputs [17–19].

Material properties of polysilicon	
Thickness	3.5 μm
Electrical resistivity	4.0×10^{-4} Ω-m
Thermal conductivity	150 W/m-K
Poisson ratio	0.29
Modulus of elasticity	165 GPa
Coefficient of thermal expansion	3×10^{-6}/K
Yield strength	1.2 GPa
Density	2.33×10^{3} kg/m^3

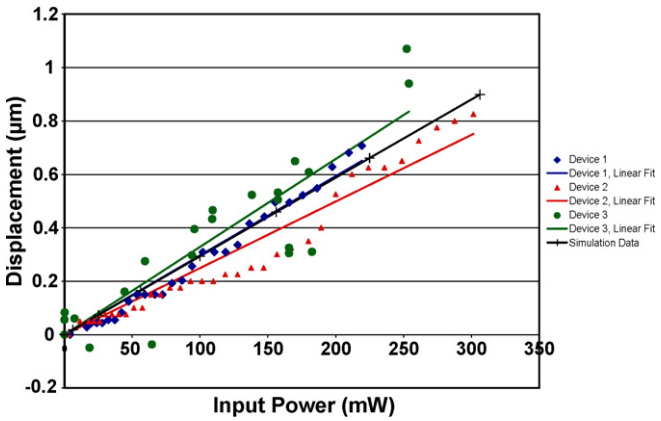

Fig. 3. Data and linear regression fit lines for three test platforms, used to derive values for *B*, the proportionality constant between input power and unconstrained displacement. Also plotted in this figure is data from a simulation of displacement versus input voltage squared, indicating a linear relation for the simulated system with constant thermal and electrical conductivities. The simulated data has been scaled by a factor of 2 to fit on the plot of experimental data, because the simulated data does not include losses due to the polysilicon connections between the contact pads and the actuator on the chip.

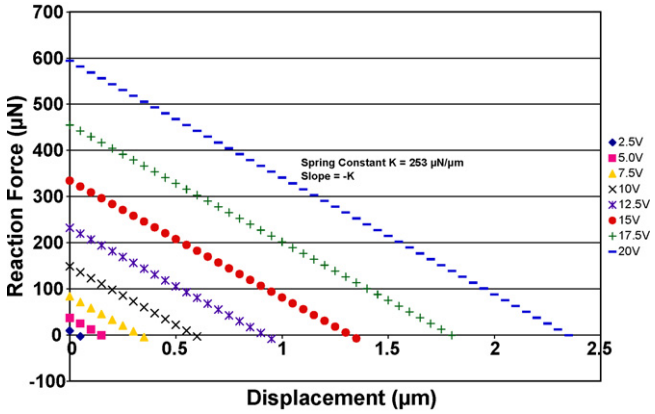

Fig. 4. Simulation output of the reaction force at the tip of the stage for different values of actuator voltage and constraints on the tip displacement.

rated from the actuator and mechanically anchored. For example, at 15 V the simulation predicts a stage temperature of 229 °C, as seen in Fig. 5. This is significantly lower than the actuator temperature of 437 °C, but it demonstrates a need for further optimization of the thermal design.

2.3. Mechanical measurements

Tensile measurement is enabled by fixing a material specimen across the gap between the moving and fixed portions of the stage. The experiment reported here uses scanning electron microscope (SEM) observation as a direct means of measuring the stage displacement and carbon nanofiber strain. Microscopy requires the interpretation of micrographs in order to derive strain data, which can be a slow process. Sensors could provide a faster approach to acquisition of strain data, and to that end, several indirect strain measurement mechanisms were built into the reported device. These mechanisms can be seen at left in Fig. 2, and as built in the center of Fig. 1. They include a diffraction grating, a piezoresistive beam bending sensor, and an electron emission or gas ionization sensor. All require further characterization. The diffraction grating is designed to measure stage displacement using a reflected laser beam. The electron or ion sensor concept is based on a comparison of electron or ion current arriving at fixed and moving electrodes. For piezoresistive measurements, electrical current is carried in two of the polysilicon anchoring beams. Motion of the stage bends the beams, thereby modifying the electrical resistance of each beam.

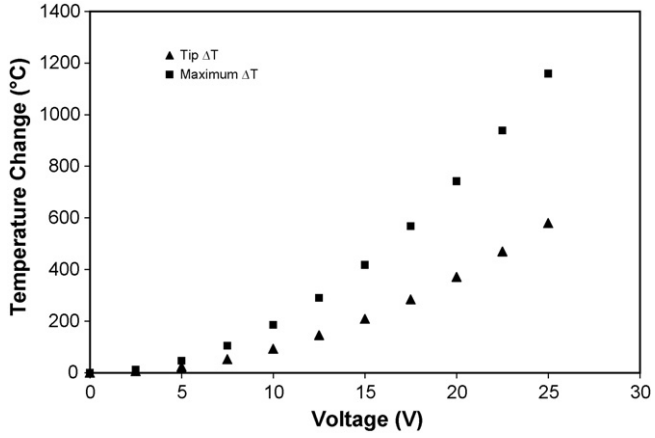

Fig. 5. Thermal simulation results from ANSYS simulation. Plot of maximum temperature change, which is located in the actuators, and the temperature change of the tip of the moving stage at various voltage inputs to the actuator.

This concept has been explored in Ref. [20], but further development is required to ensure that resistivity changes are due to piezoresistive rather than thermal effects. The successful implementation of one of the displacement sensors above can be used in combination with bending of a beam of known stiffness to measure a force output to the fiber, as in the approach taken in Ref. [8]. This direct force measurement has not yet been implemented in our design.

2.4. Force calibration

Calibration of force applied to the nanofiber specimen can be derived indirectly from measurement of actuator input power and stage displacement. The simulation shown in Fig. 4 indicates that at any given applied voltage, there is a linear relation between force and displacement. In essence, the beams in the actuator and the beams that stabilize the stage act as a spring. At every input power level, the spring and actuator system equilibrates itself to accommodate the expansion of the beams within the actuator and a steady-state thermal dissipation of power from the actuator. Displacement perturbation in the vicinity of this mechanical equilibrium exhibits a linear force versus displacement behavior, which can be described with a spring constant K. Force F can be estimated by comparing measured stage displacement d with the displacement d_0 that is expected for a given power input:

$$F = K(d_0 - d)$$

The simulation in Fig. 4 estimates $K = 253\ \mu N/\mu m$. When an analytical estimate is performed, modeling the spring constant as the sum of the spring constant of perpendicular clamped–clamped beams of varying lengths, and including the beams in the actuator, a value of 293 μN/μm is obtained for K, which is in the vicinity of the value from the simulation. If the temperature dependence of polysilicon electrical and thermal conductivity is included in the simulation, as in Ref. [14], the force versus displacement behavior diverges from linearity, although it is still linear in the vicinity of the free stage displacement. The magnitude of slope of these curves increases at higher electrical power inputs, indicating that the spring constant K is power dependent and that K from the constant conductivity simulation likely underestimates the highest forces.

The expected displacement d_0 can be estimated from calibration based on the input power to the actuators. By measuring the behavior of a freely moving system, the interplay of electrical, thermal, and mechanical behavior is incorporated into the fitting parameters that relate d_0 to the input power P. ($P = IV$, the current flowing through the actuator times the voltage drop across the actuator.) As seen in Fig. 3, measurements of displacement d_0 versus power P on unconstrained stages give linear fits according to the following equation:

$$BP = d_0$$

From these measurements, the linear regression fitting constant B lies in the range of 0.0024 to 0.0034 (μm/mW), with R^2 (coefficient of determination) values ranging from 0.82 to 0.97. For the data presented in Fig. 3, Devices 1 and 2, a power law fit provides a slight improvement to these R^2 values (respectively, 0.985 and 0.947 for the power law fit versus 0.974 and 0.954 for the linear fit). Because the fitting improvement is only slight for these data series and because the power law fit does not improve the fit to the data from Device 3, the linear fit appears to serve adequately for the data presented here. With improvement in measurement, power-law curve-fitting remains a strategy to further refine the force calibration.

Current and voltage supplied to the actuators were predominantly measured using two point electrical measurements. A

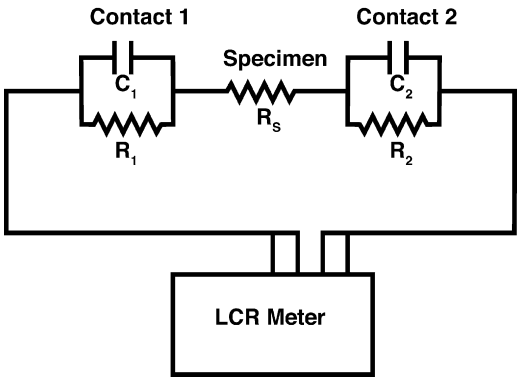

Fig. 6. Circuit diagram for a fiber specimen with amorphous carbon contacts. Each contact has contact resistance R_1 and R_2, and contact capacitance C_1 and C_2. For fiber piezoresistive measurements, the resistance of the fiber R_s must be resolved.

comparison of two point and four point measurements found less than 3% mismatch in actuator resistance values between these methods. From these measurements, it can be inferred that the resistance in the actuator circuit is dominated by the actuator and its connections to the pads on the chip, and not bond pad contact resistance or line resistance from the power supply.

2.5. Electrical characterization

Although two gold connections for the fiber specimen have been provided on the moving stage, they are electrically linked by the underlying polysilicon layer. Two separate electrical contacts were defined on the fixed side of the stage, effectively enabling a three-point conductivity measurement. In practice, the difficulty of carbon nanofiber placement limited actual connections to only two: one on the moving stage, and one on the closest portion of the fixed stage. The fiber was mechanically clamped to the stage with amorphous carbon deposits that also served as electrical connections. The amorphous carbon contacts present a high electrical resistivity, giving contact resistances R_1 and R_2 values on the order of several megaohms.

The structure of the contacts consists of a highly resistive material in a thin layer between two more conductive materials. In essence, these contacts are capacitors with lossy dielectrics. These capacitors lie in series with the fiber specimen, whose resistance is of interest in relation to strain behavior. Capacitors in a series circuit create a high-pass filter. At low frequencies and for direct currents (dc), current must flow directly through the contacts and is therefore limited by the high resistance of the amorphous carbon contacts. As the frequency of an alternating current (ac) increases, the capacitors at the fiber contact points will begin to behave as if the contacts were shorted. Current at higher frequencies will capacitively couple across the contact points and thereby minimize the effect of the contact resistance on the impedance. (Fig. 6) The fiber resistance and the reactance due to the contact capacitances will therefore dominate the measured impedance.

The electrical connection to the moving stage is made by a bending polysilicon beam with a gold layer patterned on top of the beam. The conductivity of the gold dominates that of the polysilicon, so current flows predominantly in the gold layer. Therefore, the piezoresistive change experienced by the polysilicon beam can be neglected. The circuit probing the nanofiber resistance R_s and the contact resistances R_1 and R_2 has some inherent resistance of about 5 Ω. However, the small cross-section of the nanofiber implies that R_s has a value on the order of kilo-ohms, so R_s, R_1, and R_2 dominate the circuit resistance.

The circuit to the fiber specimen has inductance L which may reduce the magnitude of the observed reactance. Inductive reactance X_L is proportional to angular frequency ω and inductance. ($X_L = \omega L$) Capacitive reactance X_C is inversely proportional to angular frequency ω and capacitance C. ($X_C = -1/\omega C$) When both inductance and capacitance are small, and the ac frequency is kept relatively low (below the MHz range), the capacitive reactance will have a much larger value than the inductive reactance, and therefore dominates the reactance measurement.

2.6. Electrical connections

Three electrical circuits are tied together by the moving stage. These are the thermal actuator circuit, the nanofiber resistance measurement circuit, and, if desired, a displacement measurement circuit through bending polysilicon beams. If these circuits are not tied together at any other point, for instance if no more than one of the circuits is grounded, then the three circuits can operate independently.

3. Experiment

The microdevice was fabricated from polysilicon with Au contacts using the PolyMUMPs service. [13] The polysilicon layers were released using a 3 min etch in 48% $HF_{(aq)}$ followed by supercritical CO_2 drying.

Carbon nanotube (CNT) core carbon nanofibers were synthesized at the University of Colorado in Boulder using Fe catalyst in a chemical vapor deposition (CVD) reactor at 725 °C; they were subsequently ultrasonicated for 3 h in a toluene solution and dried to form a mat. A three-axis piezoelectric micro-manipulator (Kleindiek™) with a tungsten microscopy probe was used for separating an individual nanofiber from the mat. The synthesis and nanotube separation procedures were the same as the ones detailed in Ref. [21]. The nanofiber was then transferred and bonded at its ends to the MEMS tensile stage by performing electron beam-induced deposition (EBID) for 10 min in a JEOL JSM-6480LV SEM operated in spot mode with 30 kV acceleration voltage. The device substrate was bonded to a chip carrier, with wire-bonding for electrical connections, and this system was mounted in the SEM.

A variable dc power supply provided electrical current to the thermal actuator. Voltage and current supplied to the actuators were measured using a Hewlett Packard 34401A multimeter. Using an Agilent 4263B LCR meter, the nanofiber resistance and reactance were observed during mechanical loading. The stage displacement and nanofiber length were extracted from SEM images using ImageJ software. High-resolution scanning electron microscopy was performed using a JEOL JSM-7401F field emission SEM, operating at 1.8 kV acceleration voltage.

4. Results and discussion

4.1. Actuator

During operation of the actuator at constant voltage, the electrical resistivity was sometimes observed to decline after the voltage was set at each new level, and similar fluctuation was observed in Ref. [22]. Furthermore, observation (Fig. 7) of actuator electrical resistivity during the carbon nanofiber mechanical test described below indicated that the actuators experienced increased resistance with increasing electrical power inputs, and different electrical resistance values during unloading versus loading, possibly due to piezoresistive effects on the actuators, as has been elaborated in Ref. [22]. Because the actuator electrical resistance varies during an experiment, calibration based on voltage inputs alone is insufficient to predict the unconstrained displacement of the stage, which depends on the thermal resis-

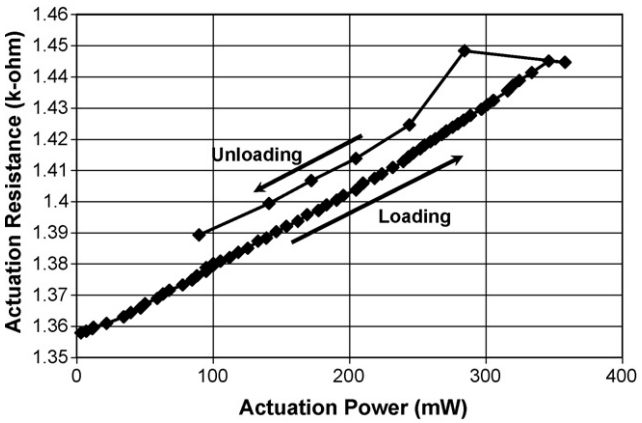

Fig. 7. During the experiment, the polysilicon actuator shows a linear increase in electrical resistance with increasing input power, with a small resistivity hysteresis upon reduction of the input power.

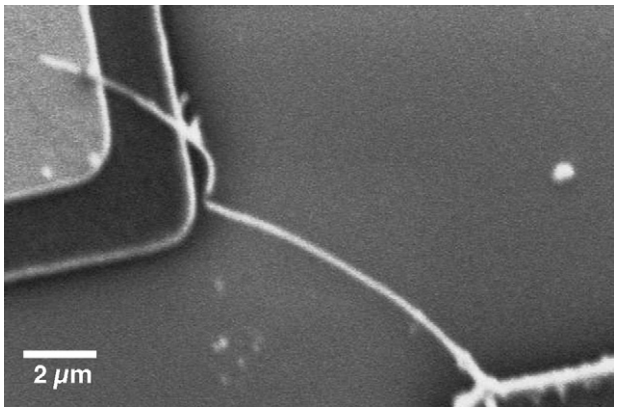

Fig. 9. Image of the nanofiber after the moving stage has returned to its original position.

tance, power dissipation, and thermal expansion of the actuator beams.

4.2. Carbon nanofiber

Before loading, dc resistance across the carbon nanofiber was >10 MΩ. However, measurement at 100 kHz found 5.0 kΩ resistance and −55.5 kΩ reactance, indicating that contact resistance dominates the dc measurement. The negative reactance indicates that the reactance is dominated by the capacitance. If the capacitance is inferred from the total reactance, the measured reactance corresponds to an inline capacitance of 28.7 pF, or 57.4 pF at each contact if the contacts are assumed to be identical. Measurement at 10 kHz gave 44 pF inline capacitance. No significant trends in the nanofiber resistance or reactance were observed in the subsequent tensile test, likely indicating that current in the fiber was predominantly carried by outer layers of the fiber without a great degree of piezoresistance.

As the nanofiber was loaded, first it straightened and simultaneously elongated, until direct tensile load was applied to the entire length of the fiber. Failure eventually occurred in the outer layers of the fiber as seen in Fig. 8. As the moving stage was allowed to return to its original position, the nanofiber buckled upon it as seen in Fig. 9, indicating that the failure seen in Fig. 8 was not a complete fracture. In Figs. 10 and 11 it can be seen that only a portion of the strain could be recovered as the fiber was unloaded, indicating that the nanofiber experienced a plastic deformation.

Using the force calibration approach defined above, the stage displacement and actuator input power measurements were mapped into estimates of the force applied to the CNT. In order to calculate the engineering stress applied to the fiber, the fiber diameter was measured using high-resolution SEM imaging, as seen in Fig. 12. For the value of B, the fitting parameter from Device 3, which was from the same PolyMUMPs [13] fabrication run as the device used to obtain the carbon nanofiber data in Fig. 3, was used. The value of B was scaled to account for a greater expected displacement than in the calibration device due to beams that did not survive the HF release process. The fitting parameter, $B = 0.00557$ μm/mW, had a 6% standard error from the calibration data for Device 3, and most of the other sources of error in the related measurements (such as stage displacement, voltage, and current measurements, and variation in the dimensions of the beams of the released actuators) were also within this amount. Better understanding of the accuracy of this force calibration method will be enabled by additional calibration experiments measuring the microsystem spring constant and the expected displacement of devices subjected to different etch conditions during the release step of processing.

Fig. 11 shows the stress–strain response as the fiber straightened and started to take the load along its length. Because typically the outer diameter $D_o \gg D_i$, the inner CNT diameter, for these nanofibers, the loading stress can be estimated by assuming a coreless geometry [21], using $D_o = 140$ nm (Fig. 12). The initial portion of the curve shows the typical linear elastic deformation behavior observed in CNTs and similar materials. A linear fit to the initial portion of the curve (up to 4% strain) yields a slope or Young's modulus value of ∼350 GPa. This value falls well within the experimental values reported in the literature [3,8]. It should be noted that the CNTs used in this study had amorphous coating (as thick as 30 nm) surrounding its outer shell, due to excess reaction gas pyrolysis during the CNT synthesis. The amorphous carbon greatly degrades the mechanical properties as compared to pristine CNTs (which can have a Young's modulus value as high as 1 TPa).

Further extension of the nanofiber to ∼5% strain resulted in permanent damage to its outer shells, giving rise to plastic behavior

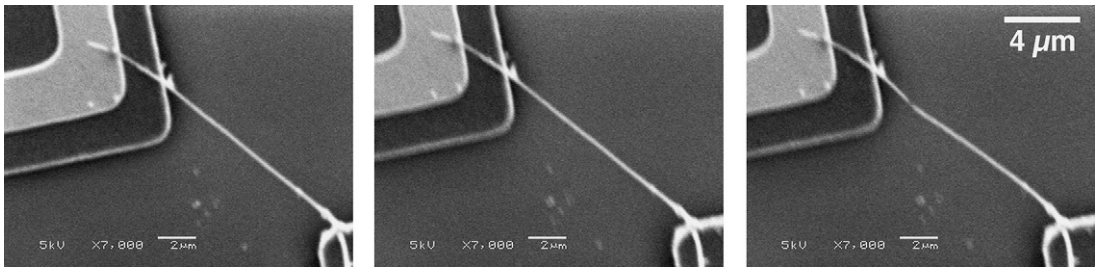

Fig. 8. Tensile observation. Left: slack removed from nanofiber before significant loading, $R = 5.01$ kΩ (measured at 100 kHz). Center: nanofiber just before failure, $\varepsilon = 5.3\%$. $R = 4.98$ kΩ. Right: failure of an outer layer. $R = 4.98$ kΩ. Reactance values ranged from $X = -54.7$ kΩ to -57.0 kΩ. No significant trends in resistance or reactance were observed for this sample during the tensile test.

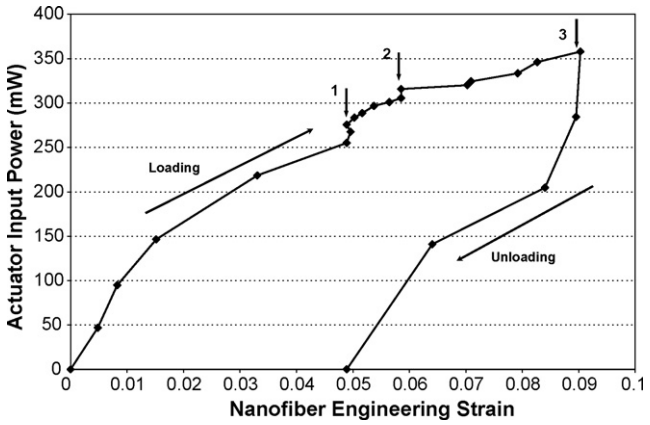

Fig. 10. Strain was determined from extension of the nanofiber from its length when completely unloaded. Following from the origin, the three marked inflection points indicate (1) where the fiber had straightened, (2) a point where the specimen resistance changed spontaneously under a constant strain, and (3) the point just after failure, seen at right in Fig. 7, where the fiber began to be unloaded.

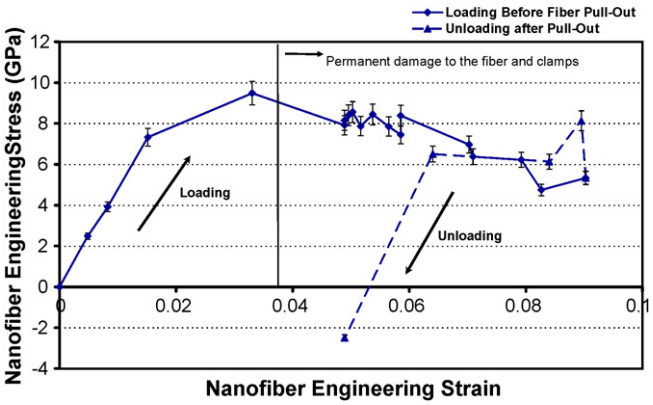

Fig. 11. Estimates of stress and strain applied to the carbon nanofiber during loading and unloading. These estimates were derived from calibration of the test device according to the input power applied to the actuator, and the measured displacement of the stage. Error bars show 6% error based on known error in calibration of the system.

until the outer shell eventually fractured and the inner nanotube nearly pulled out (Fig. 12). As seen in Fig. 9, the fiber buckled when the stage was returned to a point of zero input power, and this has manifested as a small amount of compressive stress observed in the final data point of the tensile test in Fig. 11.

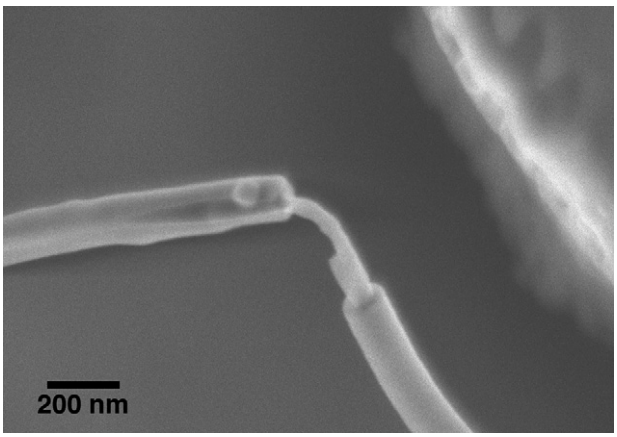

Fig. 12. High-resolution SEM micrograph of the failure "neck" in the carbon nanofiber. In this image it is evident that a 43 nm carbon nanotube core has pulled out from the 140 nm carbon fiber, which appears to have fractured during the mechanical testing.

Subtraction of the nanofiber length change from the stage displacement provides a measurement of slippage or elastic deformation in the clamps. In the elastic portion of the tensile curve, the displacement in the clamps increases, but then remains approximately constant (0.38 ± 0.06 μm) in the plastic portion of the tensile curve while nanofiber strain increased. It is not surprising that there should be some deformation within the clamps, because clamp failure was commonly observed in bending experiments reported by Singh et al. [23] using the same carbon nanofibers and clamping techniques.

5. Conclusions

A stage for electromechanical testing of micro- and nanoscale fibers has been designed, simulated, and fabricated. The stage was used for electrical measurements continuously during a mechanical tensile test of a carbon nanofiber.

The use of ac two-point impedance measurements has been demonstrated as a means to bypass the high contact resistance from mechanical welds to electrically conducting tensile specimens.

For carbon nanofiber testing, specimens were placed using a micromanipulator and bonded using amorphous carbon deposited in an SEM. The development of faster approaches to displacement measurement and to nanofiber placement is needed to improve the quality of mechanical characterization data of nanoscale fibers. By measuring the stage displacement and actuator input power, the stress applied to a carbon nanofiber during a tensile test was estimated. A typical telescopic mode of failure involving breaking of outer shells was realized.

Acknowledgements

The studies conducted by the authors from the University of Colorado - Boulder, the University of Texas - Austin, and Northwestern University are supported by the DARPA Center on Nanoscale Science and Technology for Integrated Micro/Nano-Electromechanical Transducers (iMINT), funded by the DARPA N/MEMS S&T Fundamentals Program (award #HR0011-06-1-0048). This research is based upon work supported under a National Science Foundation Graduate Research Fellowship, which supports J.J. Brown. The authors wish to thank NIST-Boulder and Paul Rice at the University of Colorado for help with the nanotubes and the micromanipulator. Additionally, the authors thank Dr. Christofer Hierold, and Dr. Alain Jungen, ETH Zurich, Micro- and Nanosystems, for many fruitful discussions about subjects related to this research.

References

[1] A. Jungen, C. Stampfer, J. Hoetzel, V.M. Bright, C. Hierold, Process integration of carbon nanotubes into microelectro-mechanical systems, Sensors Actuat. A 130 (2006) 588.
[2] C. Stampfer, A. Jungen, C. Hierold, Fabrication of discrete nanoscaled force sensors based on single-walled carbon nanotubes, IEEE Sensors J. 6 (2006) 613.
[3] M.F. Yu, O. Lourie, M.J. Dyer, K. Moloni, T.F. Kelly, R.S. Ruoff, Strength and breaking mechanism of multiwalled carbon nanotubes under tensile load, Science 287 (2000) 637.
[4] M.-F. Yu, B.S. Files, S. Arepalli, R.S. Ruoff, Tensile loading of ropes of single wall carbon nanotubes and their mechanical properties, Phys. Rev. Lett. 84 (2000) 5552.
[5] S. Lu, D.A. Dikin, S. Zhang, F.T. Fisher, J. Lee, R.S. Ruoff, Realization of nanoscale resolution with a micromachined thermally actuated testing stage, Rev. Sci. Inst. 75 (2004) 2154.
[6] S. Lu, Z. Guo, W. Ding, R.S. Ruoff, Analysis of a microelectromechanical system testing stage for tensile loading of nanostructures, Rev. Sci. Inst. 77 (2006) 056103.
[7] M. Kiuchi, S. Matsui, Y. Isono, Mechanical characteristics of FIB deposited carbon nanowires using an electrostatic actuated nanotensile testing device, J. MEMS 16 (2007) 191.

[8] Y. Zhu, A. Corigliano, H.D. Espinosa, A thermal actuator for nanoscale *in situ* microscopy testing: design and characterization, J. Micromech. Microeng. 16 (2006) 242.
[9] A. Jungen, C. Meder, M. Tonteling, C. Stampfer, R. Linderman, C. Hierold, MEMS actuator for integrated carbon nanotube strain sensing, in: Proceedings of 2005 IEEE Sensors, Vols. 1 and 2, Irvine, CA, USA, October 31 to November 3, 2005, pp. 93–96.
[10] A. Jungen, L. Durrer, C. Stampfer, C. Hierold, Nanoscale straining of individual carbon nanotubes by micromachined transducers, in: Solid-State Sensors, Actuators and Microsystems Conference, 2007. TRANSDUCERS 2007, June 10–14, 2007, pp. 1561–1564.
[11] P.A. Williams, S.J. Papadakis, M.R. Falvo, A.M. Patel, M. Sinclair, A. Seeger, A. Helser, R.M. Taylor II, S. Washburn, R. Superfine, Controlled placement of an individual carbon nanotube onto a microelectromechanical structure, Appl. Phys. Lett. 80 (2574) (2002) 2576.
[12] J.J. Brown, J.W. Suk, G. Singh, D.A. Dikin, R.S. Ruoff, V.M. Bright, Microsystem for electromechanical measurements of carbon nanofiber loading and failure, in: SSSAMW-08 Proceedings of the 2008 Hilton Head Workshop in Solid State Sensors, Actuators, and Microsystems, Hilton Head, SC, USA, June 2008, pp. 182–185.
[13] PolyMUMPS Service, MEMSCAP, Inc., Research Triangle Park, NC, USA.
[14] J.W. Wittmer, M.S. Baker, L.L. Howell, Simulation, measurement, and asymmetric buckling of thermal microactuators, Sensors Actuat. A 128 (2006) 395.
[15] L. Que, J.-S. Park, Y.B. Gianchandani, Bent beam electrothermal actuators. Part I. Single beam and cascaded devices, J. MEMS 10 (2001) 247.
[16] Y. Zhang, Q.-A. Huang, R.G. Li, W. Li, Macro-modeling for polysilicon cascaded bent beam electrothermal microactuators, Sensors Actuat. A 128 (2006) 165.
[17] T. Moulton, G.K. Ananthasuresh, Micromechanical devices with embedded electro-thermal-compliant actuation, Sensors Actuat. A 90 (2001) 38.
[18] C.-S. Oh, W.N. Sharpe Jr., Techniques for measuring thermal expansion and creep of polysilicon, Sensors Actuat. A 112 (2004) 66.
[19] W.N. Sharpe Jr., B. Yuan, R. Vaidyanathan, R.L. Edwards, Measurements of Young's modulus, Poisson's ratio, and tensile strength of polysilicon, in: Proceedings of IEEE MEMS 97, 1997, pp. 424–429.
[20] T.L. Waterfall, G.K. Johns, R.K. Messenger, B.D. Jensen, T.W. McLain, L.L. Howell, Observations of piezoresistivity for polysilicon in bending that are unexplained by linear models, Sensors Actuat. A 141 (2008) 610.
[21] G. Singh, P. Rice, K.E. Hurst, J.H. Lehman, R.L. Mahajan, Laser-induced exfoliation of amorphous carbon layer on an individual multiwall carbon nanotube, Appl. Phys. Lett. 91 (2007) 033101.
[22] T.L. Waterfall, K.B. Teichert, B.D. Jensen, Simultaneous on-chip sensing and actuation using the thermomechanical in-plane microactuator, J. MEMS 17 (2008) 1204.
[23] G. Singh, P. Rice, R. McIntosh, R.L. Mahajan, Fabrication and mechanical characterization of carbon nanotube based nanoknives, in: Proceedings of ASME IMECE2006, Chicago, IL, USA, 2006, p. 14659.

Biographies

Joseph J. Brown received an M.S. in Mechanical Engineering from the University of Colorado at Boulder in May 2008, and an A.B. in Engineering Sciences from Dartmouth College (Hanover, NH) in 2000. He has worked at Los Alamos National Laboratory (Los Alamos, NM) and at several small companies in New Hampshire, where he helped found NanoComp Technologies, Inc. (Concord, NH), a carbon nanotube manufacturer. He is currently pursuing a Ph.D. in Mechanical Engineering at the University of Colorado at Boulder with interests in materials processing, and nanoscale characterization and patterning.

Gurpreet Singh completed his Bachelors in Mechanical Engineering from Government College of Engineering Pune, India in 2003. He received his M.S. and Ph.D. degrees in Mechanical Engineering from the University of Colorado at Boulder in 2006 and 2007, respectively. He is currently a post-doctoral associate and group leader in nano-bio-devices at the Institute for Critical Technology and Applied Science (ICTAS) at Virginia Tech (Blacksburg, VA). His research interests include fabrication and mechanical characterization of thin film composites and carbonaceous materials for application in engineering and life sciences.

Ji Won Suk received the B.S. and M.S. degrees in Mechanical and Aerospace Engineering from Seoul National University, Seoul, Korea in 2000 and 2003, respectively. He was a researcher at LG Chem./Research Park in Daejeon, Korea from 2003 to 2007, where he focused on a plastic lab-on-a-chip, microfluidics and microfabrication. He is currently pursuing a Ph.D. degree in Mechanical Engineering at the University of Texas at Austin with interests in nanoscale fabrication and characterization with application to nano-electro-mechanical systems (NEMS).

Alicia I. Baca received her B.S. in Mechanical Engineering from the University of New Mexico (Albuquerque, NM) in the fall of 2007. While studying at UNM, she also worked at Sandia National Laboratories for two and a half years as a technical intern in the MEMS Packaging department. At the University of Colorado, she is pursuing a Master's degree in Mechanical Engineering, focusing on the assembly of nanoscale materials into MEMS structures.

Dmitriy A. Dikin received his Ph.D. degree from the Institute for Low Temperature Physics and Engineering at Kharkov, Ukraine in 1992. From 1992 to 1993, he was a Postodoctoral Fellow at Physics Institute, University of Würsburg, Germany. Currently, he is Research Professor at the Northwestern University, Evanston, IL. His research activities include study of physical and mechanical properties of nanotubes and nanowires, prototype NEMS device assembly, low noise electrical measurements, ultra-low and variable temperature measurements, electron microscopy and surface analysis. Dikin is a co-author of more than 60 refereed journal articles in the field of physics, mechanics, and material science.

Rodney S. Ruoff is a member of the faculty at the University of Texas at Austin, where he serves as a Cockrell Family Regents Chair in Mechanical Engineering. Prior to joining UT-Austin, Rod Ruoff served as Director of the Biologically Inspired Materials Institute at Northwestern University. He has been a 'Visiting Chair Professor' at Sungkyunkwan University in South Korea. He received his B.S. in Chemistry from the University of Texas (Austin) and Ph.D. from the University of Illinois-Urbana, in 1988. He was a Fulbright Fellow at the Max Planck Institute-Goettingen, Germany. From 1989 to 1990, he was a Postdoctoral Fellow at the IBM T.J. Watson Research Center in New York. Prior to joining Northwestern in 2000, he was a Staff Scientist at the Molecular Physics Laboratory of SRI International and Associate Professor of Physics at Washington University. His research activities include global environment and energy; synthesis and physical/chemical properties of nanostructures and composites; nanorobotics, NEMS, and developing new tools for biomedical research. Prof. Ruoff has published ~180 refereed journal articles in the fields of chemistry, physics, mechanics, and materials science.

Victor M. Bright received his BSEE degree from the University of Colorado at Denver in 1986, and the M.S. and Ph.D. degrees from the Georgia Institute of Technology, in 1989 and 1992, respectively. Dr. Bright is currently the Alvah and Harriet Hovlid Professor of Mechanical Engineering and the Faculty Director for Discovery Learning, College of Engineering and Applied Science (CEAS), University of Colorado at Boulder. From 2005 through 2007, he served as the Associate Dean for Research, CEAS, CU-Boulder. Prior to joining the University of Colorado, he was a Professor in the Department of Electrical and Computer Engineering, Air Force Institute of Technology, Wright-Patterson Air Force Base, Ohio (1992–1997). During 2004 he was a Visiting Professor at the Swiss Federal Institute of Technology (ETH-Zurich), Switzerland. Prof. Bright's research activities include micro- and nano-electro-mechanical systems (MEMS and NEMS), silicon micromachining, microsensors/microactuators, opto-electronics, optical, magnetic and RF microsystems, atomic-layer deposited materials, ceramic MEMS, MEMS reliability, and MEMS packaging. Dr. Bright has served on the Executive Committee of the ASME MEMS Division, on the Technical Program Committee of the IEEE MEMS 2000 through 2006 conferences, and as the General Co-Chair for the IEEE MEMS 2005 International Conference. He also served on the Technical Program Committee for the Transducers'03, Transducers'07 and IEEE/LEOS Optical MEMS 2003 through 2005. He taught a Short Course on MEMS Packaging at Transducers'03 and Transducers'05. Prof. Bright is a Senior Member of IEEE, a Fellow of ASME, and an author of over 250 journal papers, conference proceedings, and book chapters in the fields of MEMS, NEMS and microsystems. He is a Section Editor for the Micromechanics Section of the Journal Sensors and Actuators A: Physical.